Chemical genetic approaches for target validation
Wel, T. van der

Citation
Wel, T. van der. (2020, January 22). *Chemical genetic approaches for target validation.* Retrieved from https://hdl.handle.net/1887/83257

Version:	Publisher's Version
License:	[Licence agreement concerning inclusion of doctoral thesis in the Institutional Repository of the University of Leiden](#)
Downloaded from:	[https://hdl.handle.net/1887/83257](#)

Note: To cite this publication please use the final published version (if applicable).

Cover Page

Universiteit Leiden

Author: Wel, T. van der
Title: Chemical genetic approaches for target validation
Issue Date: 2020-01-22

5

Towards a chemical genetic strategy

for subtype-selective inhibition

of diacylglycerol lipase alpha

Introduction

Endocannabinoids are essential signaling lipids in the brain and are involved in regulation of various physiological processes, ranging from learning and memory to appetite and emotion.[1–3] Unlike polar neurotransmitters, which are typically released from vesicles, signaling lipids such as endocannabinoids appear to be synthesized on demand.[4,5] This implies that the cellular machinery involved in endocannabinoid homeostasis plays an essential role in signaling processes. Spatiotemporal endocannabinoid action is therefore likely controlled by a dynamic network including the enzymes for their biosynthesis and degradation.

The diacylglycerol lipases alpha and beta (DAGLα and β) are serine hydrolases responsible for the biosynthesis of the signaling lipid 2-arachidonoylglycerol (2-AG), the most abundant endogenous ligand for the cannabinoid (CB) type 1 receptor in the brain.[6] Despite relatively low overall homology (34% identical amino acids), both enzymes share a multi-pass integral membrane domain as well as a catalytic domain with a typical α/β hydrolase fold and Ser-His-Asp catalytic triad[6,7] (Figure 5.1A). Interestingly, DAGLα possesses an additional domain at the carboxy-terminal tail with multiple (putative) phosphorylation sites[8] as well as a Homer protein-binding PPxxF motif.[9,10] DAGLα and DAGLβ both catalyze the hydrolysis of diacylglycerols (DAGs) at the *sn*-1 position to generate monoacylglycerols (MAGs), implying that the active sites of these two DAGL enzymes likely have high structural similarity (Figure 5.1B).
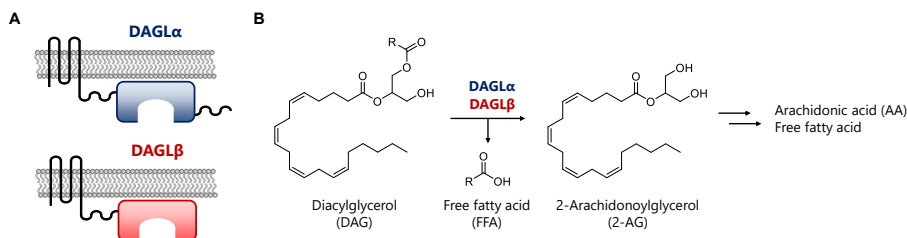

Figure 5.1 – Diacylglycerol lipase alpha and beta synthesize 2-arachidonoylglycerol from diacylglycerols. (A) DAGLα and DAGLβ share a multi-pass integral membrane domain as well as a catalytic domain with a typical α/β hydrolase fold and Ser-His-Asp catalytic triad. In addition, DAGLα possesses a unique carboxyl-terminal tail. **(B)** Both subtypes catalyze the hydrolysis of diacylglycerols (DAGs) at the *sn*-1 position to generate monoacylglycerols such as 2-arachidonoylglycerol (2-AG).

Despite this resemblance in substrate catalysis, both DAGL subtypes appear to have distinct physiological functions. Animal models with genetic deletion of either DAGL have provided valuable insight in the relative contribution of each subtype in 2-AG biosynthesis. For example, DAGLα knockout (KO) mice have 80% lower 2-AG levels in the brain, whereas these levels were decreased by 50% in DAGLβ[KO] counterparts. On the other hand, liver 2-AG levels were more drastically altered in DAGLβ[KO] than DAGLα[KO] mice (90%

versus 60% reduction, respectively).[11] Although this indicates that both subtypes cannot completely compensate for each other's loss, it cannot be ruled out that long-term congenital deletion of one DAGL subtype might be partially compensated by the other variant on the transcriptome or proteome level. In addition, DAGL expression is dynamically controlled during neuronal development. DAGLα, for example, is highly expressed in neurons, whereas DAGLβ is more abundant in microglia.[12] Although advanced genetic techniques allow for cell type-specific gene knockouts, these models lack the temporal control required to investigate the individual roles of the DAGL subtypes in this dynamic process.[13]

Long-term compensation effects can be avoided using acute inactivation of DAGL activity via pharmacological tools. Indeed, blockade of DAGL activity by small-molecule inhibitors with an α-ketoheterocycle (LEI-105) or triazole urea scaffold (DH376 and DO34) rapidly reduced 2-AG levels in cells and the central nervous system, respectively.[14,15] However, currently available DAGL inhibitors target both DAGLα and DAGLβ. Subtype selectivity by medicinal chemistry efforts has proven to be exceptionally challenging to achieve, in part due to a lack of a crystal structure of the active site of DAGLα and DAGLβ, which impedes structure-based inhibitor design. Moreover, achieving cellular specificity, *i.e.* targeting one specific cell type in the brain, such as neurons or microglia, remains a major challenge with pharmacological tools. This hampers the validation of both enzyme subtypes as a therapeutic target for various diseases, such as metabolic disorders and neurodegenerative diseases.[16–18]

The field of chemical genetics combines the specificity of genetics with acute modulation of enzyme activity by small-molecule inhibitors. Garske *et al.* previously introduced the concept of covalent complementarity for protein kinases. Chapters 2, 3 and 4 of this thesis demonstrated that mutagenesis of active site residues into a reactive cysteine allows the development of covalent, mutant-specific inhibitors. A similar chemical genetic approach comprised of a DAGLα cysteine mutant and complementary inhibitor would be ideally suited to achieve subtype-selective inhibition of DAGLα. In addition, cell type-specific incorporation of mutant DAGLα using mouse genetics techniques would allow for acute modulation of DAGLα exclusively in a specific cell type, without affecting wild-type DAGLα expressed in other cell types.

This chapter describes the first steps towards the development of a chemical genetic strategy to identify a DAGLα cysteine mutant that can be selectively targeted by a complementary inhibitor. Leu651, directly following catalytic His650 of the catalytic triad, was identified as a position in the DAGLα active site that can be mutated into a cysteine with limited effects on catalytic activity and enzyme kinetics. Next, a complementary inhibitor was synthesized that covalently and irreversibly reacted with this cysteine, is selective for DAGLα[L651C] and does not target wild-type DAGLα nor DAGLβ. However, a

biphasic binding behavior was observed, which indicated that only ~50% of the enzyme population was available for covalent addition to the complementary inhibitor. Further optimization is thus required to obtain a chemical genetic toolbox suitable to dissect subtype-specific roles of DAGLα and DAGLβ or modulate DAGLα activity with cellular specificity.

Results

Design and biochemical characterization of DAGLα cysteine mutants

The active site of DAGLα and DAGLβ recognizes similar substrates and performs similar chemical reactions. Available inhibitors generally cross-react with the other subtype and are non-selective, dual DAGLα/β inhibitors (Figure 5.2A). To achieve subtype-specific inhibition of DAGLα using chemical genetics, active site residues were mutated into a cysteine: a nucleophilic amino acid with a thiol moiety that can be covalently targeted by electrophilic inhibitors (Figure 5.2B). Since DAGLβ (as well as wild-type DAGLα) lacks native cysteine residues in its active site, it is envisioned that covalent chemistry to this engineered cysteine can be exploited to improve subtype selectivity. Key to this strategy is that the catalytic activity, enzyme kinetics and substrate recognition are not abolished by the introduced mutation. This ensures minimal disturbance to normal cellular physiology when applied in living model systems, and allows for acute perturbation of the enzyme function
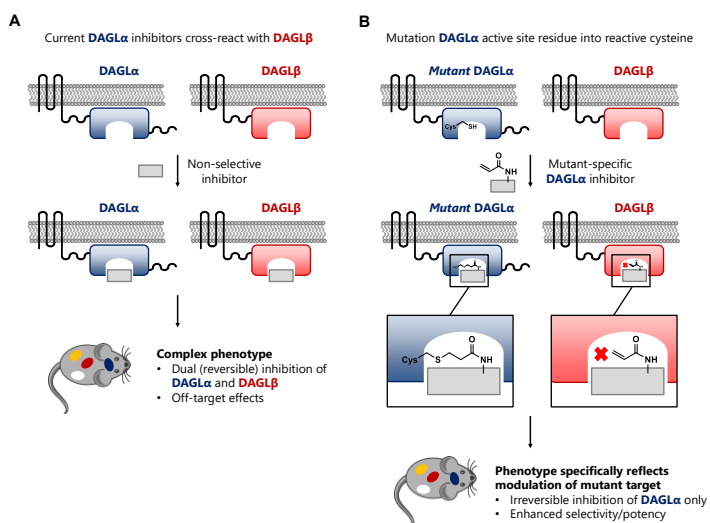

Figure 5.2 - Chemical genetic strategy for subtype-selective inhibition of DAGLα. (A) Current DAGLα inhibitors cross-react with DAGLβ, resulting in dual inhibition of both subtypes. **(B)** The presented strategy involves mutagenesis of an active site residue in DAGLα into a cysteine, accompanied by the design of a mutant-specific, complementary inhibitor that covalently and irreversibly reacts with the introduced cysteine. This covalent, irreversible binding mode enhances inhibitor potency on DAGLα and selectivity against DAGLβ, which lacks native cysteine residues in its active site.

only upon administration of the complementary, mutant-selective inhibitor. To identify an amino acid in the DAGLα active site that can be substituted for a cysteine without affecting protein function, a previously reported DAGLα homology model with docked reversible inhibitor **1** was examined.[19] Twelve amino acid residues were selected for mutagenesis, based on their location, appropriate positioning and distance to the ligand (Figure 5.3A). The corresponding DAGLα cysteine mutants were subsequently generated using site-directed mutagenesis and cloned into a mammalian expression vector in frame with a C-terminal FLAG-tag. The mutant proteins were expressed in HEK293T cells (transfections performed in triplicate), followed by cell lysis and preparation of membrane fractions which were used for further biochemical profiling.

Activity-based protein profiling (ABPP) is used to visualize active pools of enzyme in complex proteomes by reacting to specific fluorescent activity-based probes (ABPs). The set of 12 mutants was profiled using MB064, a structural analog of tetrahydrolipstatin, which targets a variety of serine hydrolases including many endocannabinoid hydrolases[19], and DH379, a more selective ABP that targets DAGLα/β and ABHD6[15] (Figure 5.3B). Quantification of labeling intensities (Figure 5.3C) revealed that three mutants (T408C, H429C and G431C) showed greatly reduced labeling intensities by both ABPs. Interestingly, these three mutants were all located in the same binding pocket in the DAGLα active site. Other mutants (M432C, G538C, L659C) exhibited a labeling intensity of approximately 50% compared to wild-type. However, various mutants (I529C, L531C, L647C, L651C and G658C) showed only minimally reduced or, in some cases, enhanced labeling intensities. Of note, MB064 and DH379 labeling intensities showed a moderate correlation (R^2 = 0.38, Figure 5.3D), with preferential labeling of some mutants by one particular probe (*e.g.* G502C by DH379 and I529C by MB064). These results highlight the benefit of using two probes with distinct chemotypes for biochemical characterization of the enzymes.

Because ABPs only label the pool of active enzymes, reductions in labeling intensity can originate from lower probe binding affinity, altered protein folding or lower mutant expression levels compared to wild-type protein. The latter was examined using immunoblot analysis against the C-terminal FLAG-tag (Figure 5.3B, E), which revealed that some mutants (G431C, M432C, G538C, L651C) indeed had lower expression levels than wild-type DAGLα, possibly due to protein misfolding and reduced stability. However, other mutants (T408C and H429C) matched wild-type expression levels, whereas no probe labeling was observed, indicating that these substitutions may directly prevent probe binding, for example by steric clash or changes in protein folding that prohibit entry of the probe into the DAGLα active site.
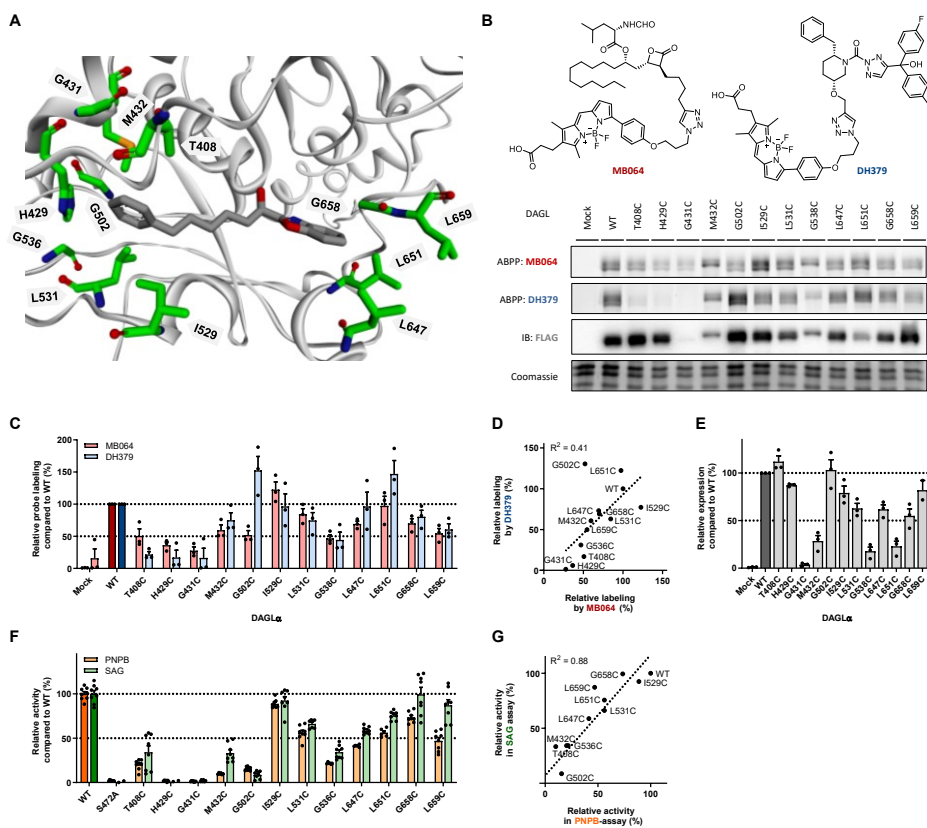
Figure 5.3 – Design of DAGLα cysteine point mutants and characterization by activity-based protein profiling and substrate assays. (A) Location of mutated active site residues in DAGLα homology model with docked reversible inhibitor **1**. **(B, C)** Recombinantly expressed DAGLα mutants analyzed by activity-based protein profiling using probes MB064 (250 nM, 15 min, rt) and DH379 (1 μM, 15 min, rt). Protein expression levels were determined by anti-FLAG immunoblot. Band intensities were normalized to wild-type control (N = 3, individual transfections). **(D)** Correlation between MB064 and DH379 labeling intensities. **(E)** Relative expression of DAGLα mutants compared to wild-type. Band intensities were corrected for protein loading and normalized to wild-type control (N = 3, individual transfections). **(F)** Biochemical activity of DAGLα mutants analyzed by surrogate (PNP-butyrate) and natural (SAG) substrate assays. Activity was determined using slope of reaction progress curve in linear range and normalized to wild-type control (N = 2, n = 4). **(G)** Correlation between relative activities determined using PNPB and SAG as substrates. Data represent means ± SEM.

Next, mutant enzyme activity was measured using two substrate-based assays employing the surrogate substrate *para*-nitrophenyl butyrate (PNPB) and the natural substrate 1-stearoyl-2-arachidonoyl-*sn*-glycerol (SAG), respectively (Figure 5.3F). Membrane preparations overexpressing DAGLα variants were incubated with the chromogenic substrate PNPB, resulting in hydrolysis of the ester bond and release of *para*-nitrophenol that can be monitored by absorbance measurements.[20] In a similar fashion, hydrolysis of the physiological substrate SAG by DAGLα results in release of 2-AG, which is indirectly converted into a fluorescent signal via a multi-enzyme cascade reaction.[21] The slopes of the corresponding reaction progress curves were determined in the linear range

and normalized to wild-type DAGLα activity. Multiple mutants (T408C, H429C, G431C, M432C, G502C and G536C) showed a more than 50% reduction of hydrolytic activity in both substrate assays (Figure 5.3F). This reduction in hydrolase activity can for some mutants (*e.g.* G431C and M432C) be ascribed to reduced expression levels. However, other inactive mutants (*e.g.* H429C) had no hydrolytic activity despite expression levels similar to wild-type, suggesting that His429 is essential for substrate binding or conversion. Activities determined in the substrate assays showed a good correlation (R^2 = 0.78) with a general trend of slightly higher activity using SAG opposed to PNPB as substrate (Figure 5.3G). Moreover, the substrate hydrolysis activity profile was relatively similar to the ABPP labeling profile, with the most prominent exception being mutant G502C, which showed completely abolished substrate hydrolysis activity, even though labeling by DH379 and MB064 was (partially) preserved.
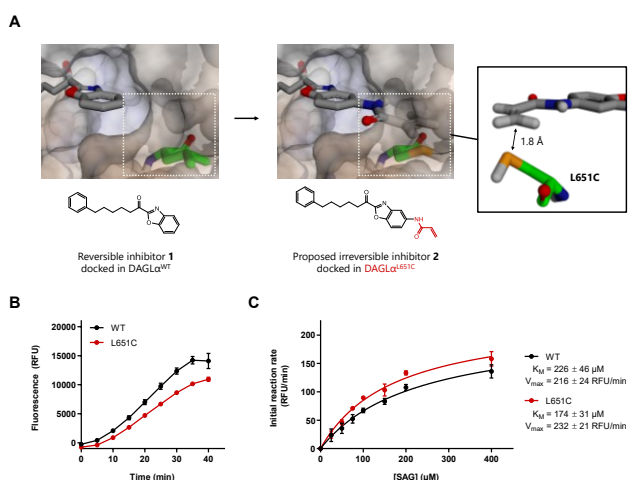

Figure 5.4 – Selection of DAGLα^L651C as catalytically active mutant for the design of complementary, irreversible inhibitors. (A) Design of a proposed irreversible inhibitor **2** to covalently target DAGLα^L651C. Installation of an acrylamide warhead on reversible inhibitor **1** positions this Michael acceptor in close proximity (1.8 Å) of the target cysteine. **(B)** Reaction progress curve of SAG hydrolysis by DAGLα^WT and DAGLα^L651C (N = 2, n = 2). **(C)** Determination of kinetic parameters K_M and V_{max} using SAG hydrolysis assay. Initial reaction rates correspond to slopes of reaction progress curves in the linear part (N = 2, n = 2). Data represent means ± SEM.

In particular, interest was drawn to a subset of mutants, *i.e.* L647C, L651C, G658C and L659C, which all retained hydrolytic activity and could be labeled by both ABPs. Furthermore, these residues are all located in the same hydrophobic pocket and in close proximity of the benzoxazole moiety of **1**. Previous structure-activity studies verified that this pocket is not completely occupied by **1** and can accommodate an additional tolyl-group[14]. It was therefore reasoned that these cysteine mutants might be targetable by an appropriately positioned electrophile on compound **1**. Of these mutants, DAGLα^L651C was expected to be most promising, since it appeared to be in close proximity (1.8 Å) and adequately positioned to react with proposed inhibitor **2** via a Michael addition reaction to its acrylamide warhead (Figure 5.4A). For this reason, DAGLα^L651C was biochemically

profiled in more detail using the SAG hydrolysis assay. DAGLα^{L651C} showed a reaction progress curve similar to DAGLα^{WT} (Figure 5.4B). Despite slightly lower SAG hydrolysis activity (76% compared to WT), its maximal reaction rate was unaffected (WT: V_{max} = 216 ± 24 RFU/min, L651C: V_{max} = 232 ± 21 RFU/min; P >0.05). In contrast, DAGLα^{L651C} showed a minor but non-significant increase in SAG binding affinity as reflected by a lower Michaelis-Menten constant (WT: K_M = 226 ± 46 µM, L651C: K_M = 174 ± 31 µM; P >0.05) (Figure 5.4C). Finally, it was confirmed that mutagenesis of Leu651 into a cysteine had no detrimental effect on the affinity of **1** (WT: pIC_{50} = 5.8 ± 0.04, L651C: pIC_{50} = 5.5 ± 0.05) (Table 5.1 and Supplementary figure 5.1).
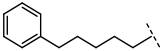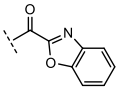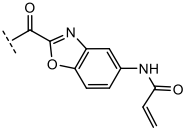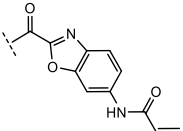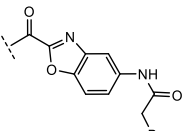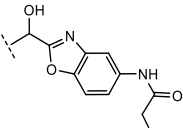
Design and synthesis of mutant-specific inhibitors

Compound **1** served as a suitable starting point for the design of mutant-specific inhibitors, since it was previously reported to have a relatively low affinity (pIC_{50} ~ 5) for DAGLα and DAGLβ.[19,22] Electrophilic derivatives were synthesized, possessing acrylamide warheads intended to react with the cysteine residues (Scheme 5.1). Compounds **2** and **3**, proposed as potential irreversible inhibitors by undergoing a Michael addition to nearby Cys651 (Figure 5.4A), did not show any increase in potency on DAGLα^{L651C} or other mutants under standard assay conditions (20 min pre-incubation, rt) (Table 5.1 and Supplementary figure 5.1). Interestingly, compound **2** showed potent inhibition (> 100-fold increase) of the engineered enzyme upon increased incubation time and elevated temperatures (60 min, 37 °C) (Figure 5.5B). This suggested that the initial lack of mutant inhibition may not be due to inappropriate positioning of the warhead on the scaffold, but is due to low reactivity of the cysteine. For this reason, compound **4** with a bromoacetamide warhead, a more reactive electrophile than the acrylamide group, was synthesized. Indeed, a marked increase in inhibitory potency was observed on DAGLα^{L651C} but not on DAGLα^{WT} compared to compound **2** under standard assay conditions (Figure 5.5A).
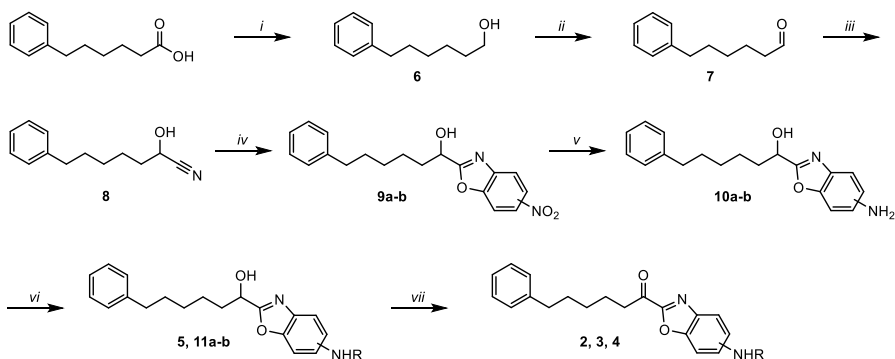
Scheme 5.1 - Synthesis towards electrophilic derivatives of compound 1. *i*) LiAlH$_4$, Et$_2$O, 0 °C, 97%. *ii*) DMSO, oxalyl chloride, DCM, -78 °C. *iii*) KCN, THF:H$_2$O (1:1), rt, 73% over 2 steps. *iv*) Acetyl chloride, EtOH, CHCl$_3$; 2-amino-4-nitrophenol (**9a**) or 2-amino-5-nitrophenol (**9b**), pyridine, EtOH, 80 °C, 30-64%. *v*) PtO$_2$, H$_2$, EtOAc, rt, 57%-quant. *vi*) Bromoacetyl bromide (**5**) or acryloyl chloride (**11a-b**), DIPEA, DCM, 0 °C, 76%-quant. *vii*) Dess-Martin periodinane, DCM, rt, 75-88%.

Table 5.1 – Inhibitory potency of synthesized compounds on DAGLα^{WT} and mutants. Shown values represent pIC$_{50}$ ± SD determined using the PNPB hydrolysis assay with 20 min pre-incubation at rt (N = 2, n = 4 for vehicle, N = 2, n = 2 for inhibitor-treated). The two values (i, ii) for compound **2** and **4** on L651C represent both pIC$_{50}$ values of the biphasic dose-response curve. † Inhibitor incubation 60 min at 37 °C.

Compound	Structure	pIC$_{50}$ WT	pIC$_{50}$ L651C
1		5.8 ± 0.04	5.5 ± 0.05
2		< 5 5.0 ± 0.07 †	5.0 ± 0.10 i) 8.3 ± 0.12 † ii) < 5 †
3		< 5	5.5 ± 0.05
4		5.9 ± 0.05	i) 8.9 ± 0.39 ii) 5.8 ± 0.19
5		4.8 ± 0.08	4.8 ± 0.03

Identification and characterization of a subtype-selective inhibitor for DAGLα^{L651C}

Notably, compound **4** (and **2** under modified conditions) displayed a biphasic IC$_{50}$ curve that was independent of assay buffer pH and reduction agent (Supplementary Figure 5.2). This biphasic curve can potentially be explained by two putative binding events of the compound: an irreversible binding event of the introduced cysteine with the bromoacetamide warhead (pIC$_{50}$ = 8.9 ± 0.39) and a reversible binding event of the catalytic serine to the α-keto group (pIC$_{50}$ = 5.8 ± 0.19). Three different experiments were performed to investigate this hypothesis. First, membranes overexpressing DAGLα were pre-incubated with iodoacetamide (IAA), an alkylating agent that irreversibly reacts with the thiol group of cysteine residues, to block the covalent reaction of Cys651 to the bromoacetamide group of compound **4**, while leaving the reactivity of the catalytic serine of the enzyme intact. Indeed, IAA pretreatment reverted the two-phase binding curve of compound **4** on DAGLα^{L651C} to a one-phase dose-response curve with a low pIC$_{50}$ similar

to reversible control compound **1** (Figure 5.5C), whereas IAA did not affect the inhibitory effect of compound **4** on DAGLα^{WT} (Figure 5.5E) or basal DAGLα activity (Figure 5.5D, F). Second, the pIC$_{50}$ of compound **4** was determined using different pre-incubation times.

This analysis revealed that the enzyme inhibition was time-dependent only for the binding event reflected by the most potent interaction, but not for lower affinity interaction (Figure 5.5G, H). Third, a displacement assay was performed using ABP MB064. Membranes overexpressing DAGLα^{L651C} were pre-incubated with **4** or reversible control inhibitor LEI105[14] at their corresponding IC$_{80}$-concentration, followed by addition of
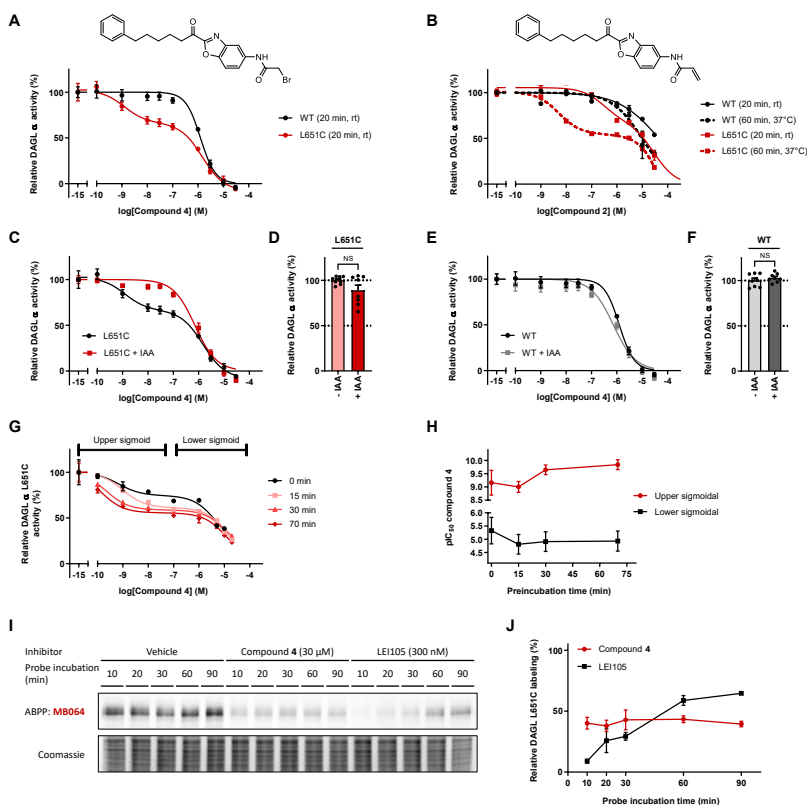

Figure 5.5 – Identification of mutant-selective, irreversible inhibitors of DAGLα^{L651C}. (A, B) Dose-response curves of compound **4** (A) and **2** (B) on DAGLα^{WT} and DAGLα^{L651C}, determined using PNPB hydrolysis assay (N = 2, n = 4 for vehicle, N = 2, n = 2 for inhibitor-treated). **(C, E)** Pre-incubation with alkylating agent iodoacetamide (IAA, 20 mM, 30 min in the dark, rt) reverts biphasic binding curve of **4** on DAGLα^{L651C} (C), but does not alter inhibition profile on DAGLα^{WT} (E). **(D, F)** IAA pre-incubation does not affect basal DAGLα activity. **(G)** Two-phase binding profile of **4** on DAGLα^{L651C} is time-dependent. Compound was pre-incubated for 0-15-30-70 min prior to addition of PNPB substrate. **(H)** pIC$_{50}$ of upper sigmoidal increases with pre-incubation time of **4**, while pIC$_{50}$ of lower sigmoidal remains constant. **(I, J)** ABP MB064 outcompetes LEI105 but not compound **4** binding over time. Compounds were pre-incubated at the respective IC$_{80}$-concentration (30 μM for **4** and 300 nM for LEI105, 20 min, rt), followed by incubation with MB064 (250 nM, 10-20-30-60-90 min, rt). Band intensities were normalized to vehicle-treated control at same time point (N = 3). Data represent means ± SEM. Statistical analysis was performed using two-tailed t-test: NS if $P > 0.05$.

MB064 for different incubation times. DAGLα[L651C] labeling did not recover after pre-incubation with **4**, whereas reversible inhibitor LEI105 showed substantial displacement (Figure 5.5I, J). Altogether, the results of these three experiments suggested that the most potent inhibitory interaction is reflecting the irreversible reaction of Cys651 with the bromoacetamide warhead, while the weaker inhibitory effect is mediated by the reversible, covalent interaction of Ser472 with the α-keto group. Strikingly, compound **5,** in which the ketone is substituted for a hydroxyl moiety, showed no inhibition of DAGLα[L651C] (Table 5.1), implying that initial binding of Ser472 to the α-keto group is essential prior to covalent bond formation with Cys651. Having established that compound **4** potently and covalently inhibits DAGL[L651C], it was investigated whether compound **4** is a subtype-selective inhibitor of DAGLα[L651C] in the presence of DAGLβ. To this end, an ABPP experiment was performed using DH379. Membranes overexpressing DAGLβ and DAGLα[L651C] or DAGLα[WT] were mixed in a various ratios, which revealed that a 1:1 ratio was most optimal to achieve efficient labeling of both DAGL subtypes (Supplementary figure 5.3). DAGLα/β mixtures were then pre-incubated with different concentrations of compound **4** or LEI105, a reversible, potent dual DAGL inhibitor with related chemical structure[14] (Figure 5.6A). Quantification of the labeling intensities confirmed that LEI105 does not discriminate between DAGLα and DAGLβ, with equipotent inhibition on both subtypes (Figure 5.6B). However, the chemical genetic strategy employing DAGLα[L651C] and compound **4** allowed for selective inhibition of DAGLα in presence of DAGLβ (Figure 5.6C). Of note, a similar biphasic dose-response curve was observed in this ABPP experiment, verifying that this phenomenon was not assay-dependent.
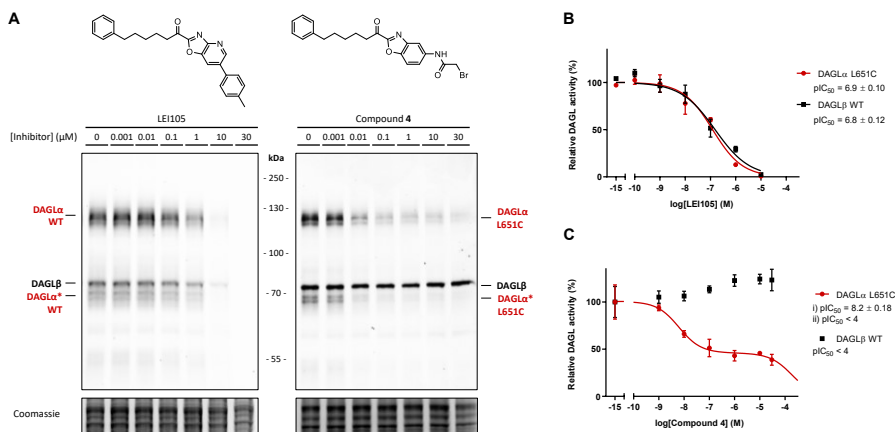
Figure 5.6 – Chemical genetic strategy allows subtype-selective inhibition of DAGLα in presence of DAGLβ. (A-C) Membranes overexpressing DAGLα[WT] or DAGLα[L651C] and DAGLβ (2 mg/mL) were mixed (1:1 ratio) and incubated with LEI105 or **4** (20 min, rt), followed by addition of DH379 (1 µM, 15 min, rt). DAGLα band marked with asterisk corresponds to a previously reported degradation product.[19] Band intensities were normalized to vehicle-treated control (N = 3). Data represent means ± SEM.

Discussion and conclusion

Previously reported DAGL inhibitor chemotypes, such as the α-ketoheterocycles[14], glycine sulfonamides[23] and 1,2,3-triazole ureas[15,24], are all dual DAGLα/β inhibitors. Exclusive targeting of one subtype has proven difficult to achieve so far. This chapter describes the first steps towards a chemical genetic strategy that allows for subtype-selective targeting of DAGLα in presence of the structurally and functionally similar DAGLβ subtype. This approach employs mutagenesis of a DAGLα active site residue into a reactive cysteine that can be selectively targeted by a complementary, covalent inhibitor.

Homology model-directed mutant design and comprehensive biochemical characterization using ABPP and substrate hydrolysis assays led to the identification of Leu651 as a suitable residue for mutagenesis into a cysteine, since DAGLα[L651C] retained its catalytic activity and kinetic properties, ensuring minimal interference to normal cellular physiology if introduced in host systems. Follow-up experiments would involve mutagenesis of this residue in an endogenous model system such as cell lines or mice using the CRISPR/Cas9 gene editing technology.[25–27] This circumvents the use of overexpression systems and allows subtype-selective targeting of DAGLα[L651C] under the appropriate epigenetic control. Mouse genetics techniques, such as Cre-LoxP recombination combined with brain cell-specific promoters[28], can be applied to introduce the engineered DAGLα protein in specific brain regions. This would enable acute pharmacological modulation of DAGLα activity exclusively in selected cell populations, for example cortical neurons or cerebellar Purkinje cells, without affecting DAGLα (and DAGLβ) activity in other neuronal cell types in the brain.

Compound **4** was identified as a mutant-specific inhibitor of DAGLα[L651C], which displayed biphasic binding behaviour that may reflect the presence of two warheads in the inhibitor. The most potent inhibitory interaction is likely the result of the irreversible, covalent reaction of Cys651 with the bromoacetamide electrophile, while the weaker inhibitory effect is mediated by the reversible, covalent interaction of catalytic Ser472 to the α-keto group. Currently, it is unknown why the engagement of the thiol does not result in complete inhibition of the enzyme, but levels off at approximately 50%. It may indicate that there are possibly two proteoforms of DAGLα[L651C], of which one possesses a non-reactive cysteine, for example due to oxidation. The thiol group of cysteine is known to be prone to oxidation, either by formation of disulfides, sulfur oxyacids or S-nitroso-species.[29] None of these oxidized cysteine species possess a reactive thiol for nucleophilic chemistry, resulting in a mixture of two DAGLα[L651C] proteoforms of which only one is potently inhibited by compound **4**. However, the biphasic binding behavior could not be reverted by incubation with various reducing agents *in vitro*. Alternatively, it is possible that DAGLα[L651C] exists as a homodimer that undergoes a conformational change upon inhibitor

binding, rendering the other monomer insusceptible to inhibition by **4**. Additional studies are required to explain these results.

In summary, this study describes the first steps towards a chemical genetic strategy that potentially allows for subtype-selective or cell type-specific inhibition of DAGLα. Residue Leu651, located directly upstream of the catalytic triad His650, was identified as a suitable position to mutate into a cysteine without substantially affecting DAGLα enzymatic activity and kinetics. Structure-based design led to the discovery of compound **4** as a mutant-selective, complementary DAGLα^{L651C} inhibitor that displays irreversible binding characteristics and can selectively target DAGLα^{L651C} in presence of DAGLβ. Further optimization of compound **4** and investigation of its biphasic binding behavior are required to obtain a chemical genetic toolbox suitable for dissecting subtype-specific roles of DAGLα and DAGLβ in endogenous model systems.

Acknowledgments

Experimental procedures - Biochemistry

General
All chemicals and other reagents were purchased from Sigma Aldrich, unless stated otherwise. Assay enzymes (glycerol kinase from *Cellulomonas sp.,* product code G6142; glycerol-3-phosphate oxidase from *Streptococcus thermophilus*, product code G4388; horse radish peroxidase from *Horseradish,* product code 77332) were purchased from Sigma Aldrich. 1-Stearoyl-2-arachidonoyl-*sn*-glycerol was purchased from Cayman Chemicals.

Cloning
Full-length wild-type human DAGLα and mouse DAGLβ cDNA was obtained from Source Bioscience and cloned into pcDNA3.1 expression vectors as previously described.[19] Mutations were introduced using Phusion site-directed mutagenesis kit (Thermo Fisher). Briefly, target plasmid was amplified by PCR using two phosphorylated primers that anneal back to back to the plasmid, of which one contains the desired mutation. The product was then circularized by blunt-end ligation with T4 DNA ligase and transformed to XL10-Gold competent cells (prepared using *E. coli* transformation buffer set; Zymo Research). Mutant plasmids were isolated using plasmid isolation kits following the supplier's protocol (Qiagen). All constructs were verified by Sanger sequencing (Macrogen).

Supplementary Table 1 – List of oligonucleotide sequences.

ID	Name	Sequence	ID	Name	Sequence
P1	DAGL-a_T408C_forw	CCCAAGGATGCCCTGTGTGACCTGACGGGTGAT	P13	DAGL-a_L531C_forw	GTCCCCAGGATTGGCTGCTCTCAGCTGGAAGGC
P2	DAGL-a_T408C_rev	GGACAGGGTCCCCCGGATACTGATC	P14	DAGL-a_L531C_rev	GAGGTCTTTGCCCAGAACCACAGCA
P3	DAGL-a_H429C_forw	GGCACCTGGCTGGGCTGCAAGGGTATGGTCCTC	P15	DAGL-a_G536C_forw	CTCTCTCAGCTGGAATGCTTCCGCAGACAGCTC
P4	DAGL-a_H429C_rev	GTGGTGCCCCTCCACGGGGAGGCGC	P16	DAGL-a_G536C_rev	GCCAATCCTGGGGACGAGGTCTTTG
P5	DAGL-a_G431C_forw	TGGCTGGGCCACAAGTGTATGGTCCTCTCAGCT	P17	DAGL-a_L647C_forw	ATCTCGCCAGCCATGTGTCATGAGCACCTGCCC
P6	DAGL-a_G431C_rev	GGTGCCGTGGTGCCCCTCCACGGGG	P18	DAGL-a_L647C_rev	GATCACCTCATTGAAGGCCTTGTTG
P7	DAGL-a_M432C_forw	CTGGGCCACAAGGGTTGCGTCCTCTCAGCTGAG	P19	DAGL-a_L651C_forw	ATGCTGCATGAGCACTGTCCCTATGTGGTCATG
P8	DAGL-a_M432C_rev	CCAGGTGCCGTGGTGCCCCTCCACG	P20	DAGL-a_L651C_rev	GGCTGGCGAGATGATCACCTCATTG
P9	DAGL-a_G502C_forw	TACTCCCCGCCAGGGTGCCTGCTGAGTGAGGAT	P21	DAGL-a_G658C_forw	TATGTGGTCATGGAGTGTCTCAACAAGGTGCTG
P10	DAGL-a_G502C_rev	GGCAAAGCACTTGAGGGTCGGATAC	P22	DAGL-a_G658C_rev	GGGCAGGTGCTCATGCAGCATGGCT
P11	DAGL-a_I529C_forw	GACCTCGTCCCCAGGTGTGGCCTCTCTCAGCTG	P23	DAGL-a_L659C_forw	GTGGTCATGGAGGGGTGCAACAAGGTGCTGGAG
P12	DAGL-a_I529C_rev	TTTGCCCAGAACCACAGCAGTCACG	P24	DAGL-a_L659C_rev	ATAGGGCAGGTGCTCATGCAGCATG

Cell culture
HEK293T (human embryonic kidney) cells were obtained from ATCC and tested on regular basis for mycoplasma contamination. Cultures were discarded after 2-3 months of use. Cells were cultured at 37 °C under 7% CO_2 in DMEM containing phenol red, stable glutamine, 10% (v/v) heat-inactivated newborn calf serum (Seradigm), penicillin and streptomycin (200 µg/mL each; Duchefa). Medium was refreshed every 2-3 days and cells were passaged two times a week at 80-90% confluence. One day prior to transfection, HEK293T cells were transferred from confluent 10 cm dishes to 15 cm dishes. Before transfection, medium was refreshed (13 mL). A 3:1 mixture of polyethyleneimine (PEI; 60 µg/dish) and plasmid DNA (20 µg/dish) was prepared in serum-free medium (2 mL) and incubated for 15 min at rt. The mixture was then dropwisely added to the cells, after which the cells were grown to confluence in 72 h. Cells were then harvested by suspension in PBS, followed by centrifugation (200 *g*, 5 min). Cell pellets were flash-frozen in liquid nitrogen and stored at -80 °C until membrane fraction preparation.

Membrane fraction preparation
Cell pellets were thawed on ice and homogenized by polytron (20,000 rpm, 3 x 7 s; SilentCrusher S, Heidolph) in lysis buffer A (20 mM HEPES pH 7.2, 2 mM DTT, 250 mM sucrose, 1 mM $MgCl_2$ and 25 U/mL benzonase). Suspensions were incubated on ice for 30 min to yield total lysates. For preparation of membrane fractions, total lysates were subjected to ultracentrifugation (93,000 *g*, 30 min, 4 °C; Beckman Coulter, Ti70 or Ti70.1 rotor) and pellets were homogenized in storage buffer B (20 mM HEPES pH 7.2, 2 mM DTT) by polytron (20,000 rpm, 1 x 10 s). Protein concentrations were determined

using Quick Start™ Bradford Protein Assay (Bio-Rad). Membrane preparations were frozen in liquid nitrogen and stored at -80 °C until use.

PNP-butyrate hydrolysis assay

Assays were performed in 50 mM HEPES pH 7.0 in clear, flat-bottom 96-well plates (Greiner). Inhibitors were added from 40x concentrated stock solution in DMSO. DAGLα-overexpressing membrane preparations (10 µg per well) were incubated with inhibitor for 20 min at rt in a total volume of 190 µL. Next, 10 µL substrate solution (PNP-butyrate in 1:1 mixture of DMSO/H_2O, final concentration 300 µM) was added. Absorbance at 420 nm was measured at 37 °C in 1 min intervals for 20 min on a GENios plate reader (Tecan). Final assay concentrations: 50 ng/µL DAGLα-overexpressing membranes, 300 µM PNP-butyrate, 5% DMSO in a total volume of 200 µL. All measurements were performed in N = 2 (individual plates), n = 2 (technical replicates on same plate) or N = 2, n = 4 for controls, with Z' ≥ 0.6.

SAG hydrolysis assay

Assays were performed in HEMNB buffer (50 mM HEPES pH 7.4, 1 mM EDTA, 5 mM $MgCl_2$, 100 mM NaCl, 0.5% (w/w) BSA) in black, flat-bottom 96-well plates (Greiner). Inhibitors were added from 40x concentrated stock solution in DMSO. A substrate solution of 1-stearoyl-2-arachidonoyl-*sn*-glycerol was prepared just prior to use. The SAG stock solution (10 mg/mL in methyl acetate) was dried under argon and subsequently taken up in 50 mM HEPES buffer (pH 7.0) + 0.75% (w/w) Triton X-100. The substrate solution was mixed to form an emulsion and stored on ice until use. DAGLα-overexpressing membrane preparations (10 µg per well) were incubated with inhibitor for 20 min at rt in a total volume of 100 µL. Next, 100 µL assay mix containing monoacylglycerol lipase (MAGL), glycerol kinase (GK), glycerol-3-phosphate oxidase (GPO), horse radish peroxidase (HRP), adenosine triphosphate (ATP), Amplifu™Red and 1-stearoyl-2-arachidonoyl-*sn*-glycerol (SAG) was added. Fluorescence (λ_{ex} = 535 nm, λ_{em} = 595 nm) was measured at rt in 5 min intervals for 60 min on a GENios plate reader (Tecan). Final assay concentrations: 5 ng/µL MAGL-overexpressing membranes, 0.2 U/mL GK, GPO and HRP, 125 µM ATP, 10 µM Amplifu™Red, 150 µM SAG, 5% DMSO, 0.0075% (w/w) Triton X-100 in a total volume of 200 µL. For IC_{50} determinations, assays were performed with variable inhibitor concentrations. For K_M determinations, assays were performed with variable SAG concentrations and fluorescence was measured at rt in 2 min intervals for 60 min on a CLARIOstar plate reader (BMG Labtech). All measurements were performed in N = 2 (individual plates), n = 2 (technical replicates on same plate) or N = 2, n = 4 for controls, with Z' ≥ 0.6.

Activity-based protein profiling

Total lysates or membrane fractions (14 µL, 1.38 mg/mL) were incubated with inhibitor (0.5 µL in DMSO, 29x concentrated stock, 20 min, rt), followed by incubation with probe MB064 or DH379 (0.5 µL in DMSO, 30x concentrated stock, 15 min, rt). Reactions were quenched with 4x Laemmli buffer (5 µL, final concentrations 60 mM Tris pH 6.8, 2% (w/v) SDS, 10% (v/v) glycerol, 5% (v/v) β-mercaptoethanol, 0.01% (v/v) bromophenol blue) for 15 min at rt. Samples were resolved by SDS-PAGE on a 10% polyacrylamide gel (180 V, 75 min or 200 V, 120 min in case of DAGLα and DAGLβ mixtures). Gels were scanned using Cy3 channel settings (605/50 filter; ChemiDoc™ MP System, Bio-Rad). Fluorescence intensity was corrected for protein loading determined by Coomassie Brilliant Blue R-250 staining and quantified with Image Lab (Bio-Rad).

Immunoblot

Samples were resolved by SDS-PAGE and transferred to 0.2 µm polyvinylidene difluoride membranes by Trans-Blot Turbo™ Transfer system (Bio-Rad) directly after fluorescence scanning. Membranes were washed with TBS (50 mM Tris pH 7.5, 150 mM NaCl) and blocked with 5% milk in TBS-T (50 mM Tris pH 7.5, 150 mM NaCl, 0.05% Tween-20) for 1 h at rt. Membranes were then incubated with primary antibody in 5% milk in TBS-T (o/n at 4 °C). Membranes were washed three times with TBS-T, incubated with matching secondary antibody in 5% milk in TBS-T (1 h at rt) and then washed three times with

TBS-T and once with TBS. Imaging solution (10 mL luminol in 100 mM Tris pH 8.8, 100 µL ECL enhancer, 3 µL H_2O_2) was added and chemiluminescence was detected on ChemiDoc™ MP System. Primary antibody: monoclonal mouse anti-FLAG M2 (1:5000, Sigma Aldrich, F3156), secondary antibody: goat anti-mouse-HRP (1:5000, Santa Cruz, sc-2005).

Data analysis, statistics and software

All shown data represent means ± SEM, unless indicated otherwise. Replicates are indicated in figure legends with N for biological and n for technical replicates, respectively. For substrate hydrolysis assays, absorbance or fluorescence values were corrected for the average of the negative control (mock-membranes + vehicle; or DAGL-membranes with no SAG for Michaelis-Menten experiment). DAGLα-overexpressing (wild-type or mutant) membranes incubated with vehicle served as a positive control. Slopes of the corrected data were determined in the linear interval. The Z'-factor for each assay plate was calculated using the formula $Z' = 1 - 3(\sigma_{pc} + \sigma_{nc})/(\mu_{pc} - \mu_{nc})$ with σ = standard deviation, µ = mean, pc = positive control and nc = negative control. Plates with $Z' \geq 0.6$ were accepted for further analysis. For IC_{50} determination, slopes were normalized to the positive control and analyzed using 'Non-linear dose-response analysis with variable slope' (GraphPad Prism 7.0). For curves with clear two-phase binding behavior, data were analyzed using 'Two sites – Fit logIC50'. For K_M and V_{max} determination, data were subjected to 'Michaelis-Menten' fit (GraphPad Prism 7.0).

All modeling figures were rendered using Discovery Studio 2016 (BIOVIA). The design of compounds was based on the homology model of DAGLα with compound **1**, with the Leu651 residue manually changed into a cysteine.[19]

Experimental procedures - Chemistry

General information

All reactions were performed using oven- or flame-dried glassware and dry solvents. Reagents were purchased from Sigma-Aldrich, Acros, and Merck and used without further purification unless noted otherwise. All moisture sensitive reactions were performed under an argon atmosphere. ^{1}H and ^{13}C NMR spectra were recorded on a Bruker AV 400 MHz spectrometer at 400.2 (^{1}H) and 100.6 (^{13}C) MHz using CDCl$_3$, MeOD or CD$_3$CN as solvent. Chemical shift values are reported in ppm with tetramethylsilane or solvent resonance as the internal standard (CDCl$_3$: δ 7.26 for ^{1}H, δ 77.16 for ^{13}C; MeOD: δ 3.31 for ^{1}H, δ 49.00 for ^{13}C; CD$_3$CN: δ 1.94 for ^{1}H, δ 118.26 for ^{13}C). Data are reported as follows: chemical shifts (δ), multiplicity (s = singlet, d = doublet, dd = double doublet, td = triple doublet, t = triplet, q = quartet, m = multiplet), coupling constants J (Hz), and integration. HPLC purification was performed on a preparative LC-MS system (Agilent 1200 series) with an Agilent 6130 Quadruple MS detector. High-resolution mass spectra were recorded on a Thermo Scientific LTQ Orbitrap XL. Compound purity (> 95% unless stated otherwise) was determined by liquid chromatography on a Finnigan Surveyor LC-MS system, equipped with a C18 column. Flash chromatography was performed using SiliCycle silica gel type SiliaFlash P60 (230–400 mesh). TLC analysis was performed on Merck silica gel 60/Kieselguhr F254, 0.25 mm. Compounds were visualized using KMnO$_4$ stain (K$_2$CO$_3$ (40 g), KMnO$_4$ (6 g) in water (600 mL)) or ninhydrin stain (ninhydrin (1.5 g) in n-butanol (100 mL) and 3 mL acetic acid).

Synthesis of 6-phenylhexan-1-ol (6)

LiAlH$_4$ (13.1 mL, 26 mmol) was added to dry Et$_2$O (80 mL) at 0 °C, followed by dropwise addition of 6-phenyl hexanoic acid (1.27 g, 6.6 mmol) in dry Et$_2$O (10 mL). The mixture was allowed to warm to rt and stirred for 16 h. The reaction was quenched by sequential addition of H$_2$O (60 mL) and 1 M HCl (60 mL) and filtered over celite. The organic layer was washed with 1 M HCl (1 x 100 mL), sat. NaHCO$_3$ (1 x 100 mL) and brine (1 x 100 mL), dried over Na$_2$SO$_4$ and concentrated to obtain title compound (1.13 g, 6.3 mmol, 97%). ^{1}H NMR (400 MHz, CDCl$_3$): δ 7.32 – 7.23 (m, 2H), 7.23 – 7.12 (m, J = 7.0, 4.4, 2.7 Hz, 3H), 3.62 (t, J = 6.6 Hz, 2H), 2.61 (t, 2H), 1.69 – 1.59 (m, J = 8.9, 7.7 Hz, 2H), 1.59 – 1.51 (m, 2H), 1.48 (s, 1H), 1.44 – 1.30 (m, 4H). ^{13}C NMR (101 MHz, CDCl$_3$): δ 142.84, 128.50, 128.36, 125.73, 63.10, 36.00, 32.81, 31.56, 29.18, 25.73.

Synthesis of 6-phenylhexanal (7)

Oxalyl chloride (2.4 g, 19 mmol) was added to dry DCM (60 mL) at -78 °C, followed by dropwise addition of a solution of DMSO (2.9 g, 38 mmol) in dry DCM (20 mL). The mixture was stirred for 1 h, after which compound **6** (1.1 g, 6.2 mmol) in dry DCM (20 mL) was added dropwisely. The reaction mixture was stirred for 1 h, followed by dropwise addition of triethylamine (8.7 mL, 62 mmol). The mixture was allowed to warm to rt and stirred for 16 h, after which it was diluted with 1 M HCl (100 mL). Layers were separated and the aqueous layer was extracted with DCM (2 x 100 mL). Combined organic layers were washed with brine (200 mL), dried over Na$_2$SO$_4$ and concentrated, yielding title compound (1.1 g, 6.2 mmol, quant.). ^{1}H NMR (400 MHz, CDCl$_3$): δ 9.62 (t, J = 1.6 Hz, 1H), 7.05 – 7.17 (m, 5H), 2.51 (t, J = 7.6 Hz, 2H), 2.29 (dt, J = 1.6, 7.6 Hz, 2H), 1.50 – 1.56 (m, 4H), 1.24 – 1.28 (m, 2H). ^{13}C NMR (101 MHz, CDCl$_3$) δ 202.66, 142.38, 128.37, 128.23, 125.60, 43.79, 35.69, 31.21, 28.73, 21.89.

Synthesis of 2-hydroxy-7-phenylheptanenitrile (8)

Compound **7** (600 mg, 3.4 mmol) was dissolved in THF/H$_2$O (1:1 ratio, 100 mL) at rt, followed by addition of KCN (2.4 g, 37 mmol). The mixture was stirred for 72 h, after which H$_2$O (100 mL) and Et$_2$O (200 mL) were added and layers were separated. The aqueous layer was extracted with Et$_2$O (2 x 100 mL). Combined organic layers were washed with sat. NaHCO$_3$, H$_2$O and brine (200 mL each), dried over Na$_2$SO$_4$ and subsequently concentrated. The crude residue was purified by flash column chromatography (5% → 20% EtOAc in pentane), yielding title compound (497 mg, 2.4 mmol, 72%). ^{1}H NMR (400 MHz, CDCl$_3$): δ 7.32 – 7.23 (m, 2H), 7.21 – 7.09 (m, 3H), 4.40 (t, J = 6.8 Hz, 1H), 3.15 (s, 1H),

2.60 (t, 2H), 1.86 – 1.72 (m, J = 11.4, 7.0 Hz, 2H), 1.70 – 1.57 (m, J = 15.4, 7.6 Hz, 2H), 1.57 – 1.44 (m, 2H), 1.44 – 1.30 (m, J = 11.1, 8.9, 4.8 Hz, 2H). ^{13}C NMR (101 MHz, CDCl$_3$): δ 142.44, 128.47, 128.39, 125.82, 120.19, 61.23, 35.76, 35.06, 31.18, 28.55, 24.47.

Synthesis of 1-(6-nitrobenzo[d]oxazol-2-yl)-6-phenylhexan-1-ol (9a)

Acetyl chloride (2.8 mL, 40 mmol) was dissolved in dry EtOH/CHCl$_3$ (1:1 ratio, 4 mL) at 0 °C and stirred for 45 min, followed by dropwise addition of compound **8** (250 mg, 1.2 mmol) dissolved in dry CHCl$_3$ (2 mL). The mixture was stirred until completion monitored by TLC, after which it was allowed to warm to rt and subsequently concentrated *in vacuo* at 25 °C. The crude imidate intermediate was coevaporated with toluene (3 x 5 mL) and dissolved in dry EtOH (2 mL). Meanwhile, 2-amino-5-nitrophenol (208 mg, 1.4 mmol) and pyridine (107 µL, 1.3 mmol) were dissolved in dry EtOH (5 mL) and the mixture was stirred at 80 °C for 30 min, followed by dropwise addition of the imidate solution. The mixture was stirred at 80 °C for 16 h and concentrated. The crude residue was purified by flash column chromatography (10% → 20% EtOAc in pentane), yielding title compound as a mixture with 2-amino-5-nitrophenol, which was used as such in the next step (approximately 30% yield based on NMR).

Synthesis of 1-(6-aminobenzo[d]oxazol-2-yl)-6-phenylhexan-1-ol (10a)

The mixture containing compound **9a** was dissolved in degassed EtOAc (50 mL), followed by addition of PtO$_2$ (13 mg, 0.06 mmol). The mixture was stirred under H$_2$ atmosphere for 16 h at rt, after which it was filtered over celite and concentrated to obtain title compound (62 mg, 0.20 mmol, 17% over 2 steps). ^{1}H NMR (400 MHz, CDCl$_3$): δ 7.38 (d, J = 8.5 Hz, 1H), 7.30 – 7.19 (m, 3H), 7.19 – 7.06 (m, J = 8.9 Hz, 3H), 6.74 (d, J = 1.7 Hz, 1H), 6.62 (dd, J = 8.4, 1.9 Hz, 1H), 4.86 (t, J = 7.1, 5.9 Hz, 1H), 2.57 (t, J = 15.3, 7.7 Hz, 2H), 2.00 – 1.85 (m, 2H), 1.59 (quint, J = 15.1, 7.5 Hz, 2H), 1.53 – 1.40 (m, 2H), 1.40 – 1.31 (m, 2H).

Synthesis of N-(2-(1-hydroxy-6-phenylhexyl)benzo[d]oxazol-6-yl)acrylamide (11a)

Compound **10a** (60 mg, 0.19 mmol) was dissolved in dry DCM (10 mL) and cooled to 0 °C, followed by addition of DIPEA (33 µL, 0.19 mmol). Next, acryloyl chloride (17 mg, 0.19 mmol) in dry DCM (2 mL) was dropwisely added and the mixture was stirred until completion monitored by TLC. The reaction was quenched by addition of H$_2$O (10 mL) and layers were separated. The aqueous layer was extracted with DCM (3 x 10 mL), combined organic layers were dried over Na$_2$SO$_4$ and subsequently concentrated at 25 °C, yielding title compound (69 mg, 0.19 mmol, quant.). ^{1}H NMR (400 MHz, MeOD): δ 8.32 (d, J = 1.2 Hz, 1H), 7.94 (d, J = 13.2 Hz, 1H), 7.64 (d, 1H), 7.45 (dd, J = 8.6, 1.7 Hz, 1H), 7.28 – 7.21 (m, 2H), 7.20 – 7.10 (m, 3H), 6.48 (qd, J = 16.9, 5.9 Hz, 4H), 5.83 (dd, J = 9.4, 2.3 Hz, 1H), 4.89 (t, J = 6.8 Hz, 1H), 2.60 (t, J = 7.6 Hz, 1H), 2.05 – 1.92 (m, 1H), 1.69 – 1.60 (m, J = 14.8, 7.5 Hz, 2H), 1.59 – 1.50 (m, 2H), 1.40 (ddd, J = 20.9, 10.3, 6.2 Hz, 2H).

Synthesis of N-(2-(6-phenylhexanoyl)benzo[d]oxazol-6-yl)acrylamide (3)

Compound **11a** (81 mg, 0.24 mmol) was dissolved in DCM (8 mL), followed by addition of Dess-Martin periodinane (164 mg, 0.39 mmol). The mixture was stirred for 16 h at rt, after which sat. NaHCO$_3$ (5 mL) and 1 M Na$_2$S$_2$O$_3$ (5 mL) were added, followed by stirring for 1 h. The aqueous layer was extracted with DCM (3 x 10 mL) and the combined organic layers were washed with sat. NaHCO$_3$ and brine (both 30 mL). The organic layers were dried over Na$_2$SO$_4$ and concentrated at 25 °C. The crude residue was purified by flash column chromatography (10% → 50% EtOAc in pentane), yielding title compound (69 mg, 0.19 mmol, 79%). HRMS (ESI+) m/z: calculated for C$_{22}$H$_{22}$N$_2$O$_3$ ([M+H]): 363.17032, found: 363.17039. ^{1}H NMR (400 MHz, CDCl$_3$): δ 8.33 (s, 1H), 7.92 (s, 1H), 7.79 (d, J = 8.7 Hz, 1H), 7.48 (dd, J = 8.7, 1.9 Hz, 1H), 7.33 – 7.22 (m, 3H), 7.21 – 7.07 (m, 3H), 6.50 (dd, J = 16.8, 1.1 Hz, 1H), 6.34 (dd, J = 16.8, 10.2 Hz, 1H), 5.83 (dd, J = 10.2, 1.1 Hz, 1H), 3.20 (t, J = 7.4 Hz, 2H), 2.63 (t, 2H), 1.92 – 1.76 (m, J = 15.2, 7.5 Hz, 2H), 1.76 – 1.64 (m, J = 15.5, 7.6 Hz, 2H), 1.52 – 1.43 (m, 2H). ^{13}C NMR (101 MHz, CDCl$_3$): δ 190.12, 163.84, 157.63, 151.44, 142.57, 138.67, 137.05, 130.85, 128.96, 128.54, 128.41, 125.82, 122.38, 118.58, 103.32, 39.51, 35.85, 31.32, 28.86, 23.86.

Synthesis of 1-(5-nitrobenzo[d]oxazol-2-yl)-6-phenylhexan-1-ol (9b)

The title compound was synthesized from *2-hydroxy-7-phenylheptanenitrile* (**8**, 200 mg, 0.98 mmol) according to the procedure described for compound **9a**. The crude residue was purified by flash column chromatography (0% → 40% EtOAc in pentane), yielding title compound (214 mg, 0.63 mmol, 64%). ^{1}H NMR (400 MHz, CDCl$_3$): δ 8.54 (d, *J* = 2.2 Hz, 1H), 8.26 (dd, *J* = 9.0, 2.3 Hz, 1H), 7.60 (d, *J* = 9.0 Hz, 1H), 7.29 – 7.18 (m, 2H), 7.18 – 7.09 (m, 3H), 5.03 (t, *J* = 7.6, 5.4 Hz, 1H), 2.58 (t, 2H), 2.10 – 1.94 (m, 2H), 1.67 – 1.58 (m, *J* = 15.3, 7.5 Hz, 2H), 1.58 – 1.45 (m, 2H), 1.45 – 1.33 (m, 2H). ^{13}C NMR (101 MHz, CDCl$_3$): δ 171.29, 154.16, 145.26, 142.43, 140.88, 128.34, 128.25, 125.66, 121.32, 116.29, 111.13, 67.89, 35.78, 35.31, 31.25, 28.88, 24.92.

Synthesis of 1-(5-aminobenzo[d]oxazol-2-yl)-6-phenylhexan-1-ol (10b)

The title compound was synthesized from *1-(5-nitrobenzo[d]oxazol-2-yl)-6-phenylhexan-1-ol* (**9b**, 214 mg, 0.63 mmol) according to the procedure described for compound **10a**, yielding title compound (195 mg, 0.63 mmol, quant.). ^{1}H NMR (400 MHz, CDCl$_3$): δ 7.30 – 7.18 (m, 3H), 7.18 – 7.07 (m, 3H), 6.90 (d, *J* = 2.2 Hz, 1H), 6.62 (dd, *J* = 8.6, 2.3 Hz, 1H), 4.86 (t, *J* = 7.4, 5.6 Hz, 1H), 3.83 (s, 1H), 2.56 (t, 2H), 2.20 – 1.70 (m, 2H), 1.64 – 1.53 (m, *J* = 15.8, 7.9 Hz, 2H), 1.52 – 1.40 (m, *J* = 15.4, 9.2, 3.8 Hz, 2H), 1.40 – 1.30 (m, 2H). ^{13}C NMR (101 MHz, CDCl$_3$): δ 168.54, 144.71, 143.74, 142.70, 141.40, 128.46, 128.32, 125.69, 113.79, 110.89, 105.15, 67.98, 35.87, 35.47, 31.34, 29.01, 24.97.

Synthesis of N-(2-(1-hydroxy-6-phenylhexyl)benzo[d]oxazol-5-yl)acrylamide (11b)

The title compound was synthesized from *1-(5-aminobenzo[d]oxazol-2-yl)-6-phenylhexan-1-ol* (**10b**, 43 mg, 0.14 mmol) according to the procedure described for compound **11a**, yielding title compound (50 mg, 0.14 mmol, quant.). ^{1}H NMR (400 MHz, CDCl$_3$): δ 8.24 (s, 1H), 7.77 (s, 1H), 7.59 (d, *J* = 8.1 Hz, 1H), 7.35 (d, *J* = 8.8 Hz, 1H), 7.30 – 7.20 (m, 2H), 7.20 – 7.09 (m, 3H), 6.43 (dd, *J* = 16.9, 1.0 Hz, 1H), 6.27 (dd, *J* = 16.9, 10.2 Hz, 1H), 5.72 (dd, *J* = 10.2, 1.2 Hz, 1H), 4.91 (dd, *J* = 7.4, 5.5 Hz, 1H), 3.31 (s, 1H), 2.07 – 1.85 (m, 1H), 1.66 – 1.55 (m, 2H), 1.52 – 1.43 (m, 2H), 1.41 – 1.33 (m, *J* = 16.7, 10.2, 3.2 Hz, 2H). ^{13}C NMR (101 MHz, CDCl$_3$): δ 169.04, 164.09, 147.72, 142.67, 140.50, 134.86, 128.19, 77.48, 77.16, 76.84, 35.91, 35.48, 31.37, 29.02, 24.98.

Synthesis of N-(2-(6-phenylhexanoyl)benzo[d]oxazol-5-yl)acrylamide (2)

The title compound was synthesized from *N-(2-(1-hydroxy-6-phenylhexyl)benzo[d]oxazol-5-yl)acrylamide* (**11b**, 32 mg, 0.09 mmol) according to the procedure described for compound **3**. The crude residue was purified by flash column chromatography (0% → 100% EtOAc in pentane), yielding title compound (24 mg, 0.07 mmol, 75%). HRMS (ESI+) m/z: calculated for C$_{22}$H$_{22}$N$_2$O$_3$ ([M+H]): 363.17032, found: 363.17039. ^{1}H NMR (400 MHz, CDCl$_3$/MeOD): δ 8.37 (d, *J* = 1.8 Hz, 1H), 7.76 (dd, *J* = 8.9, 2.1 Hz, 1H), 7.63 (d, *J* = 8.9 Hz, 1H), 7.51 (s, 1H), 7.26 (dd, *J* = 10.1, 4.6 Hz, 2H), 7.21 – 7.10 (m, 3H), 6.45 (s, 1H), 6.43 (d, *J* = 1.8 Hz, 1H), 5.80 (dd, *J* = 6.7, 5.0 Hz, 1H), 3.22 (t, *J* = 7.4 Hz, 2H), 2.65 (t, *J* = 7.7 Hz, 2H), 1.94 – 1.77 (m, 2H), 1.71 (dt, *J* = 15.4, 7.6 Hz, 2H), 1.58 – 1.42 (m, 2H).

Synthesis of 2-bromo-N-(2-(1-hydroxy-6-phenylhexyl)benzo[d]oxazol-5-yl)acetamide (5)

Compound **10b** (50 mg, 0.16 mmol) was dissolved in dry DCM (5 mL) and cooled to 0 °C, followed by addition of DIPEA (28 µL, 0.16 mmol). Next, bromoacetyl bromide (32.5 mg, 0.16 mmol) in dry DCM (1 mL) was dropwisely added and the mixture was stirred until completion monitored by TLC. The reaction was quenched by addition of H$_2$O (10 mL) and layers were separated. The aqueous layer was extracted with DCM (3 x 10 mL), combined organic layers were dried over Na$_2$SO$_4$ and subsequently concentrated at 25 °C, yielding title compound (53 mg, 0.12 mmol, 76%). ^{1}H NMR (400 MHz, CDCl$_3$): δ 8.53 (s, 1H), 7.85 (s, 1H), 7.46 – 7.37 (m, 2H), 7.31 – 7.20 (m, *J* = 9.8, 6.9 Hz, 2H), 7.20 – 7.10 (m, 3H), 4.93 (dd, *J* = 7.4, 5.4 Hz, 1H), 4.02 (s, 2H), 2.58 (t, *J* = 14.3, 6.8 Hz, 2H), 2.12 – 1.88 (m, 2H), 1.74 – 1.54 (m, *J* = 11.3, 5.6 Hz, 2H), 1.54 – 1.43 (m, 2H), 1.44 – 1.32 (m, 2H). ^{13}C NMR (101 MHz, CDCl$_3$): δ 169.22, 164.27, 148.09, 142.63, 140.75, 133.95, 128.47, 128.34, 125.73, 118.74, 112.31, 110.96, 68.08, 35.89, 35.48, 31.34, 29.58, 28.99, 24.93.

Synthesis of 2-bromo-N-(2-(6-phenylhexanoyl)benzo[d]oxazol-5-yl)acetamide (4)

The title compound was synthesized from *2-bromo-N-(2-(1-hydroxy-6-phenylhexyl)benzo[d]oxazol-5-yl)acetamide* (**5**, 30 mg, 0.07 mmol) according to the procedure described for compound **3**. The crude residue was purified by flash column chromatography (0% → 50% EtOAc in pentane), yielding title compound (22 mg, 0.05 mmol, 88%). HRMS (ESI+) m/z: calculated for $C_{21}H_{21}BrN_2O_3$ ([M+H]): 429.08083, found: 429.08082. ^{1}H NMR (400 MHz, CD$_3$CN): δ 8.98 (s, 1H), 8.25 (d, *J* = 1.9 Hz, 1H), 7.68 (dt, *J* = 8.9, 5.5 Hz, 2H), 7.35 – 7.13 (m, 5H), 4.03 (s, 2H), 3.20 (t, *J* = 7.3 Hz, 2H), 2.70 – 2.61 (m, 2H), 1.87 – 1.74 (m, 2H), 1.69 (dt, *J* = 15.5, 7.6 Hz, 2H), 1.54 – 1.39 (m, 2H). ^{13}C NMR (101 MHz, CD$_3$CN): δ 190.06, 165.07, 158.33, 147.36, 142.78, 140.80, 136.21, 128.38, 128.25, 125.61, 121.34, 112.49, 111.94, 39.03, 35.25, 31.14, 29.56, 28.34, 23.18.
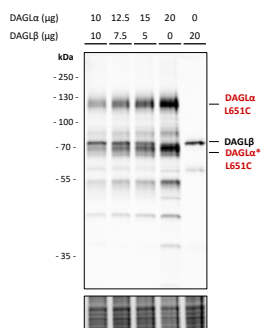
Supplementary Data
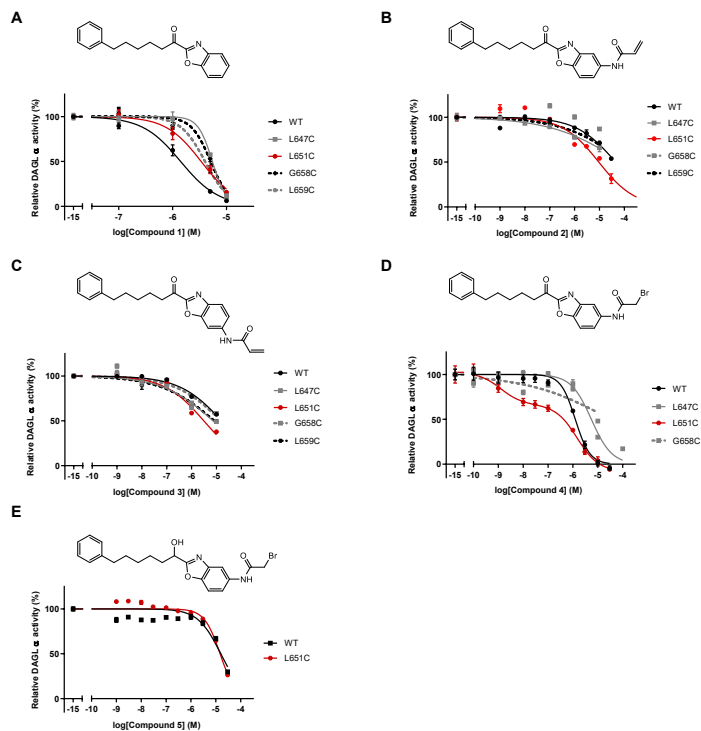
Supplementary Figure 5.1 – Dose-response curves of synthesized compounds on DAGLα^{WT} and mutants. All data were obtained using the PNPB hydrolysis assay (N = 2, n = 4 for vehicle, N = 2, n = 2 for inhibitor-treated). Corresponding pIC$_{50}$-values can be found in Table 5.1. Data represent means ± SEM.
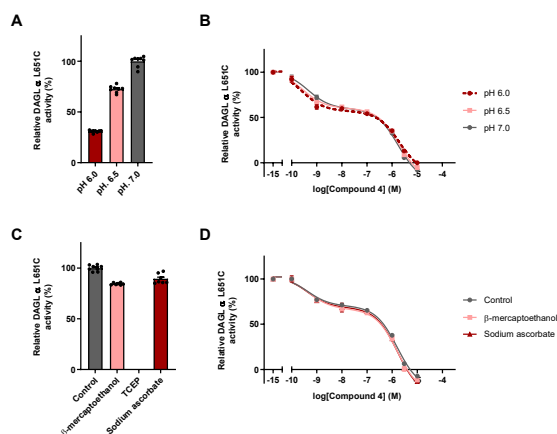
Supplementary Figure 5.2 – Biphasic binding behavior of compound 4 on DAGLα[L651C] is not pH-dependent nor affected by reducing agents. (A) Relative DAGLα[L651C] activity in buffer of different pH-values. **(B)** Dose-response curve of **4** at different pH-values. **(C)** Relative DAGLα[L651C] activity upon treatment with various reducing agents (20 mM, 30 min, 37 °C). **(D)** Dose-response curve of compound **4** after pre-incubation with reducing agents as in panel B. All data was obtained using PNPB hydrolysis assay (N = 2, n = 4 for vehicle, N = 2, n = 2 for inhibitor-treated) and represent means ± SEM.

Supplementary Figure 5.3 – Optimization of ABPP on DAGLα/DAGLβ mixtures. Membranes overexpressing DAGLα or DAGLβ (2 mg/mL) were mixed in various ratios and incubated with DH379 (1 µM, 15 min, rt). DAGLα band marked with asterisk corresponds to a previously reported degradation product.[19]

References

1. Mechoulam, R. & Parker, L. a. The Endocannabinoid System and the Brain. *Annu. Rev. Psychol.* **64**, 21-47 (2011).
2. Lutz, B. Endocannabinoid signals in the control of emotion. *Current Opinion in Pharmacology* **9**, 46–52 (2009).
3. Silvestri, C. & Di Marzo, V. The endocannabinoid system in energy homeostasis and the etiopathology of metabolic disorders. *Cell Metabolism* **17**, 475–490 (2013).
4. Alger, B. E. & Kim, J. Supply and demand for endocannabinoids. *Trends in Neurosciences* **34**, 304–315 (2011).
5. Min, R., Di Marzo, V. & Mansvelder, H. D. DAG lipase involvement in depolarization-induced suppression of inhibition: Does endocannabinoid biosynthesis always meet the demand? *Neuroscientist* **16**, 608–613 (2010).
6. Bisogno, T. *et al.* Cloning of the first sn1-DAG lipases points to the spatial and temporal regulation of endocannabinoid signaling in the brain. *J. Cell Biol.* **163**, 463–468 (2003).
7. Reisenberg, M., Singh, P. K., Williams, G. & Doherty, P. The diacylglycerol lipases: Structure, regulation and roles in and beyond endocannabinoid signalling. *Philosophical Transactions of the Royal Society B: Biological Sciences* **367**, 3264–3275 (2012).
8. Shonesy, B. C. *et al.* CaMKII regulates diacylglycerol lipase-α and striatal endocannabinoid signaling. *Nat. Neurosci.* **16**, 456–463 (2013).
9. Jung, K.-M. *et al.* A Key Role for Diacylglycerol Lipase- in Metabotropic Glutamate Receptor-Dependent Endocannabinoid Mobilization. *Mol. Pharmacol.* **72**, 612–621 (2007).
10. Murataeva, N., Straiker, A. & MacKie, K. Parsing the players: 2-arachidonoylglycerol synthesis and degradation in the CNS. *British Journal of Pharmacology* **171**, 1379–1391 (2014).
11. Gao, Y. *et al.* Loss of retrograde endocannabinoid signaling and reduced adult neurogenesis in diacylglycerol lipase knock-out mice. *J. Neurosci.* **30**, 2017–2024 (2010).
12. Viader, A. *et al.* A chemical proteomic atlas of brain serine hydrolases identifies cell type-specific pathways regulating neuroinflammation. *Elife* **5**, (2016).
13. Oudin, M. J., Hobbs, C. & Doherty, P. DAGL-dependent endocannabinoid signalling: Roles in axonal pathfinding, synaptic plasticity and adult neurogenesis. *European Journal of Neuroscience* **34**, 1634–1646 (2011).
14. Baggelaar, M. P. *et al.* Highly Selective, Reversible Inhibitor Identified by Comparative Chemoproteomics Modulates Diacylglycerol Lipase Activity in Neurons. *J. Am. Chem. Soc.* **137**, 8851–8857 (2015).
15. Ogasawara, D. *et al.* Rapid and profound rewiring of brain lipid signaling networks by acute diacylglycerol lipase inhibition. *Proc. Natl. Acad. Sci.* **113**, 26–33 (2016).
16. Di Marzo, V. Targeting the endocannabinoid system: to enhance or reduce? *Nat. Rev. Drug Discov.* **7**, 438–455 (2008).
17. Janssen, F. J. & van der Stelt, M. Inhibitors of diacylglycerol lipases in neurodegenerative and metabolic disorders. *Bioorganic Med. Chem. Lett.* **26**, 3831–3837 (2016).
18. Di Marzo, V. New approaches and challenges to targeting the endocannabinoid system. *Nature Reviews Drug Discovery* **17**, 623–639 (2018).
19. Baggelaar, M. P. *et al.* Development of an activity-based probe and in silico design reveal highly selective inhibitors for diacylglycerol lipase-α in brain. *Angew. Chemie - Int. Ed.* **52**, 12081–12085 (2013).
20. Pedicord, D. L. *et al.* Molecular characterization and identification of surrogate substrates for diacylglycerol lipase α. *Biochem. Biophys. Res. Commun.* **411**, 809–814 (2011).
21. van der Wel, T. *et al.* A natural substrate-based fluorescence assay for inhibitor screening on diacylglycerol lipase α. *J. Lipid Res.* **56**, 927–935 (2015).
22. Janssen, F. J. *et al.* Comprehensive Analysis of Structure-Activity Relationships of α-Ketoheterocycles as sn-1-Diacylglycerol Lipase α Inhibitors. *J. Med. Chem.* **58**, 9742–9753 (2015).
23. Janssen, F. J. *et al.* Discovery of glycine sulfonamides as dual inhibitors of sn-1-diacylglycerol lipase α and α/β-hydrolase domain 6. *J. Med. Chem.* **57**, 6610–6622 (2014).
24. Deng, H. *et al.* Triazole Ureas Act as Diacylglycerol Lipase Inhibitors and Prevent Fasting-Induced Refeeding. *J. Med. Chem.* **60**, 428–440 (2017).
25. Ran, F. A. *et al.* Genome engineering using the CRISPR-Cas9 system. *Nat. Protoc.* **8**, 2281–2308 (2013).
26. Cho, S. W. and Chang, H. Y. CRISPR engineering turns on genes. *Nature* **517**, 560–562 (2015).
27. Yang, H., Wu, J. J., Tang, T., Liu, K. De & Dai, C. CRISPR/Cas9-mediated genome editing efficiently creates specific mutations at multiple loci using one sgRNA in Brassica napus. *Sci. Rep.* **7**, (2017).
28. Alvarez-Castelao, B. *et al.* Cell-type-specific metabolic labeling of nascent proteomes in vivo. *Nat. Biotechnol.* **35**, 1196–1201 (2017).
29. Poole, L. B. The basics of thiols and cysteines in redox biology and chemistry. *Free Radical Biology and Medicine* **80**, 148–157 (2015).